PAPER

Check for updates

An effective H₂S sensor based on SnO₂ nanowires decorated with NiO nanoparticles by electron beam evaporation†

Tran Thi Ngoc Hoa,[a] Nguyen Duc Hoa, [ID] *[a] Nguyen Van Duy,*[a] Chu Manh Hung,[a] Dang Thi Thanh Le, [ID] [a] Nguyen Van Toan,[a] Nguyen Huy Phuong*[b] and Nguyen Van Hieu [ID] [cd]

The highly toxic hydrogen sulphide (H₂S) present in air can cause negative effects on human health. Thus, monitoring of this gas is vital in gas leak alarms and security. Efforts have been devoted to the fabrication and enhancement of the H₂S-sensing performance of gas sensors. Herein, we used electron beam evaporation to decorate nickel oxide (NiO) nanoparticles on the surface of tin oxide (SnO₂) nanowires to enhance their H₂S gas-sensing performance. The synthesised NiO–SnO₂ materials were characterised by field-emission scanning electron microscopy, transmission electron microscopy and energy dispersive spectroscopy analysis. H₂S gas-sensing characteristics were measured at various concentrations (1–10 ppm) at 200–350 °C. The results show that with effective decoration of NiO nanoparticles, the H₂S gas-sensing characteristics of SnO₂ nanowires are significantly enhanced by one or two orders compared with those of the bare material. The sensors showed an effective response to low-level concentrations of H₂S in the range of 1–10 ppm, suitable for application in monitoring of H₂S in biogas and in industrial controls. We also clarified the sensing mechanism of the sensor based on band structure and sulphurisation process.

1. Introduction

Vietnam is a developing country characterised by the growth of industrial zones and farm houses, thereby contributing to the environmental and air pollution problems.[1] The World Health Organisation reported in 2018 that approximately 60 000 annual deaths in Vietnam are linked to air pollution. Among pollutant gases, hydrogen sulphide (H₂S), a colourless, poisonous, corrosive and flammable gas with a rotten eggs smell that is mainly produced by microbial degradation of organic substances always exists in biogas.[2] However, most biogas produced in Vietnam is used without any monitoring or desulphurisation,[3] although the permissible exposure limit for 8 h time-weighted average concentration of this gas is 10 ppm as

announced by the Occupational Safety and Health Administration.[4] Monitoring H₂S gas[5] at low concentrations (ppm level) is important and the key issue in the safe usage of biogas and industrial processes.[6] Different nanomaterials and/or nanostructures have been used for H₂S monitoring,[7,8] where metal oxide-based sensors are the most popular due to their low cost, high sensitivity, compact size, real-time detection, ease of use, portability and low power consumption.[9,10,11] Tin dioxide (SnO₂) is a well-known n-type semiconductor used as a sensing material in resistive gas sensors owing to its high sensitivity for different gas species.[12] However, this material shows relatively low sensitivity to H₂S gas; thus, numerous attempts have been made to enhance its performance.[13–16] Enhancement of gas-sensing performance of metal oxides by doping[17] or surface decoration is an effective method because it can utilise the advantages of surface modulation and high catalytic activity of decorated materials.[18,19] Noble metals are generally used as decorative materials to enhance gas sensing performance, but they are expensive, leading to high cost of products.[14,20] Using other abundant materials to functionalise the surface of SnO₂ to enhance its sensing performance has becomes one of the priorities in recent years.[21,22] The common materials used to functionalise the surface of n-type SnO₂ to enhance H₂S sensing performance include p-type semiconductors, such as CuO and nickel oxide (NiO); these materials are applied to utilise the synergic effects of p–n heterojunction and catalytic activity of decorated materials.[22,23] The p-type NiO is highly reactive with

[a] International Training Institute for Materials Science (ITIMS), Hanoi University of Science and Technology (HUST), No. 1, Dai Co Viet Str., Hanoi, Vietnam. E-mail: ndhoa@itims.edu.vn; duy.nguyenvan@hust.edu.vn; Tel: +84 24 38680787; +84 24 38692963

[b] School of Electrical Engineering, Hanoi University of Science and Technology (HUST), No. 1, Dai Co Viet Str., Hanoi, Vietnam. E-mail: phuong.nguyenhuy@hust.edu.vn

[c] Faculty of Electrical and Electronic Engineering, Phenikaa Institute for Advanced Study (PIAS), Phenikaa University, Yen Nghia, Ha-Dong District, Hanoi, 10000, Vietnam

[d] Phenikaa Research and Technology Institute (PRATI), A&A Green Phoenix Group, 167 Hoang Ngan, Hanoi, 10000, Vietnam

† Electronic supplementary information (ESI) available. See DOI: 10.1039/c9ra01105f

H_2S, that is, H_2S can convert NiO into NiS;[24] thus, this material is currently used to decorate or functionalise SnO_2 to enhance its H_2S-sensing performance.[25] Several researchers have studied the decoration of SnO_2 nanomaterials by NiO nanoparticles to enhance their gas sensing performance.[26] Lee *et al.*[27] reported the improvement of H_2S sensing properties of thick-film SnO_2-based gas sensors by surface decoration with NiO and MoO_3 nanoparticles. Wet chemical pathways, such as electro-spinning[28] drop casting,[26] sol–gel[29] and hydrothermal[30,31] methods, have been used to decorate NiO on the surface of SnO_2 to enhance its gas-sensing performance. Wet chemical methods feature advantages, such as simple and low-cost fabrication, but face limitations in exact control of decoration density.[32] By contrast, electron beam evaporation is highly effective method for deposition of extremely thin NiO film over the SnO_2 layer to enhance its gas-sensing properties.[33] However, no report was conducted on the surface decoration of SnO_2 nanowires with NiO nanoparticles by electron beam evaporation for enhancement of H_2S-sensing performance, although this method is an effective technique to synthesise high-quality NiO thin films of different thicknesses.[34]

In this work, we report our study on the electron beam evaporation-based decoration of NiO nanoparticles on the surface of on-chip grown SnO_2 nanowires to enhance their H_2S gas-sensing performance. The effects of NiO thickness or density on the H_2S gas-sensing performance of SnO_2 nanowire sensors were studied. The results demonstrate that by surface decoration with NiO nanoparticles, the SnO_2 nanowire sensor showed excellent performance for monitoring low H_2S concentrations. The H_2S gas-sensing mechanism of SnO_2 nanowires decorated with NiO nanoparticles was discussed under the light of band structure and sulphurisation process.

2. Experimental

Fig. 1(A) shows the design of the gas sensor based on SnO_2 nanowires decorated with NiO nanoparticles. The sensor includes SnO_2 nanowires grown on-chip on thermally oxidised silicon substrate deposited with a pair of interdigital Pt electrodes and a thin layer of Au on top as catalyst. On the surface of SnO_2 nanowires, tiny NiO nanoparticles were decorated to modulate the conductive channel of the nanowires by electron beam evaporation followed by thermal oxidation in air. NiO is a p-type semiconductor, thus, this compound forms a p–n heterojunction after deposition on the surface of n-type SnO_2, as depicted in Fig. 1(B). H_2S gas sensor based on SnO_2 nano-wires decorated with NiO nanoparticles was fabricated by a two-step process. Firstly, SnO_2 nanowire sensor was fabricated by on-chip growth vapor–liquid–solid techniques as reported elsewhere.[35] Briefly, 0.3 g of tin (purity of 99.9%) was loaded in an alumina boat and placed at the central zone of a horizontal quartz tube furnace. Silicon substrate containing arrays of electrodes was placed 2 cm from the alumina boat. The entire system was purged with Ar (99.99%) with a flow rate of 300 sccm for 5 min, and temperature was increased at a rate of 36 °C min^{-1} from room temperature to 750 °C. The chemical vapor deposition process was subsequently carried out at
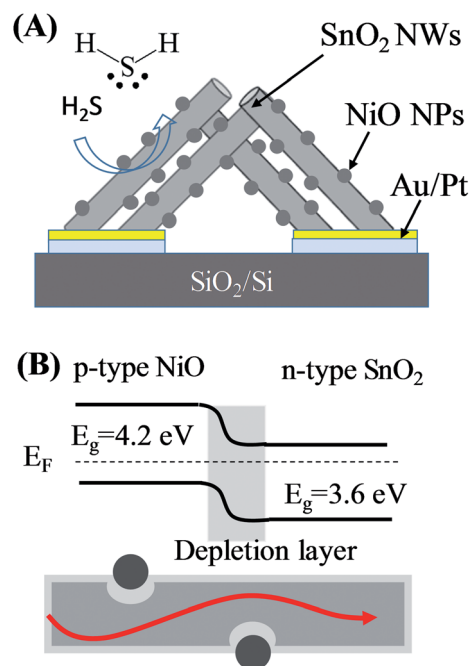

Fig. 1 (A) Design of sensor based on SnO_2 nanowires decorated with NiO nanoparticles; (B) band structure and current flow of SnO_2–NiO heterojunction.

a temperature of 750 °C with an oxygen gas flow of 0.5 sccm and pressure of 1.8×10^{-1} Torr. Growth time was maintained at 750 °C for 20 min before turning off the furnace and cooling naturally to room temperature. The SnO_2 nanowires grown by this method presented a clean surface (Fig. S1, ESI†).
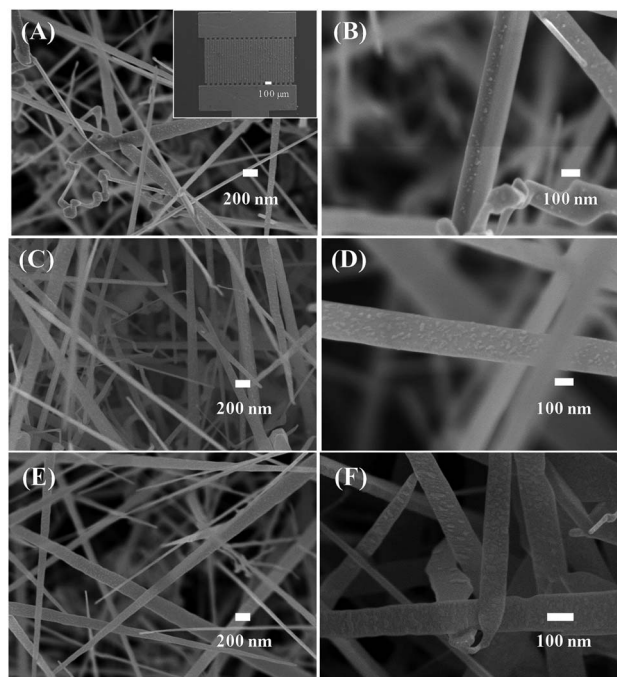

Fig. 2 SEM images of SnO_2 nanowires decorated with NiO of different thicknesses: (A and B) 3 nm; (C and D) 5 nm; (E and F) 10 nm. Inset of (A) is a SEM image of sensor device.
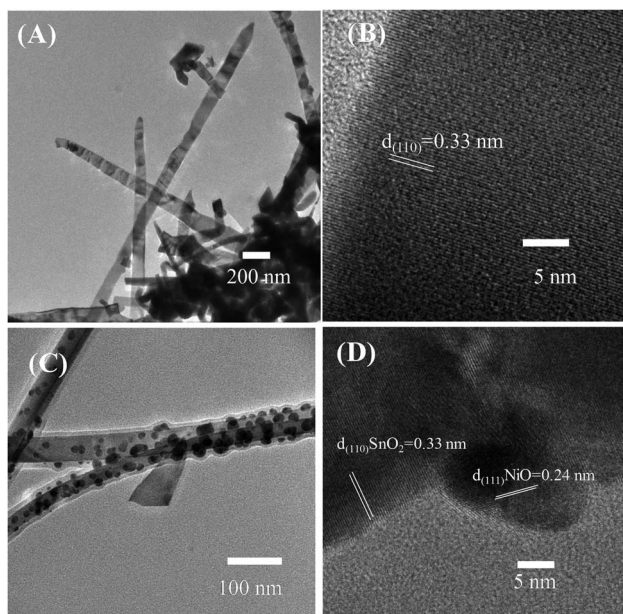
Fig. 3 Low and high magnification TEM images of (A and B) bare SnO$_2$ nanowires and (C and D) SnO$_2$ nanowires decorated with NiO nanoparticles.

After NiO nanoparticle decoration on the surface of SnO$_2$, nanowires were prepared by electron beam evaporation. Ni with three different thicknesses (thickness estimated from the deposition rate of the system) of 3, 5 and 10 nm were deposited to investigate the effect of Ni thickness on the sensing performance. The decorated samples were annealed in air at 600 °C for 3 h to convert Ni into NiO by increasing the temperature to 600 °C at a rate of 5 °C min^{-1}. The synthesised materials were studied by field-emission scanning microscopy (JEOL JSM-7600F) and transmission electron microscopy (TEM, JEM, 2100F). The gas sensing characteristics of the fabricated sensors were measured at temperatures of 200 °C, 250 °C and 300 °C by a dynamic technique as reported elsewhere.[8] During measurement, sensor resistance was continuously measured by a current-source meter (Keithley model 2602B) interfaced with a computer, whereas the gas was switched on/off from air to H$_2$S gas. The total flow rate of analytic gas was 400 sccm, whereas H$_2$S concentration varied from 1 ppm to 10 ppm.[36] Sensor response is defined as $S = R_a/R_g$, where R_a and R_g denote the resistances of the sensor in dry air and tested gas, respectively.

3. Results and discussion

3.1 Materials and gas sensing characteristics

Fig. 2 shows the low- and high-magnification SEM images of the synthesised materials. The inset in Fig. 2(A) displays the SEM image of the sensor chip, which includes two electrodes with numerous fingers of average size of is 20 μm; the gap between two fingers is 20 μm. The SnO$_2$ nanowires were grown on entirely Pt electrode fingers. The SnO$_2$ nanowire film was
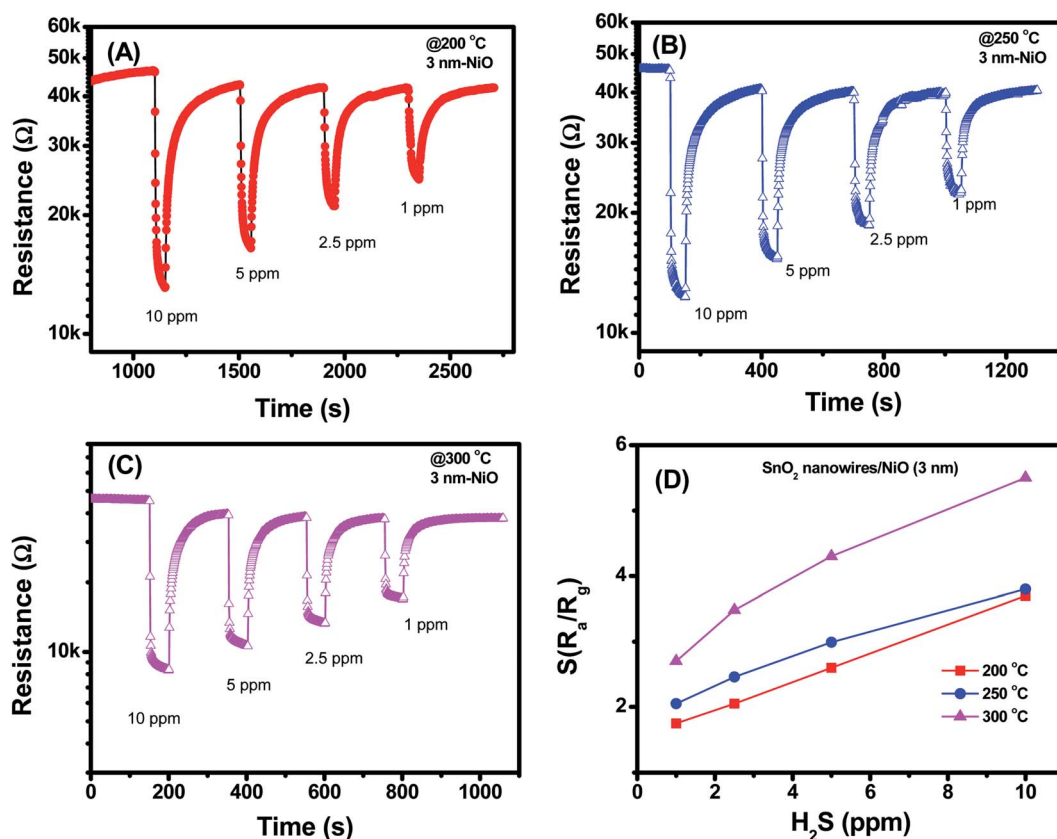

Fig. 4 H$_2$S sensing characteristics of SnO$_2$ nanowires decorated with NiO (3 nm) measured at different temperatures: (A) 200 °C; (B) 250 °C; (C) 300 °C; (D) sensor response as a function of H$_2$S concentration.

considerably thick. Thus, bare silicon substrate cannot be observed, ensuring that Ni deposition could not form a continuous layer. The SnO_2 nanowires exhibited an average size of about 100 nm. Herein, as the Au catalyst was deposited on Pt electrode, the SnO_2 nanowires featured a needle-like morphology resulting from the poor wettability of Au on Pt. After decoration with NiO, the nanoparticles were distributed homogenously on the surface of SnO_2 nanowires [Fig. 2(C and D)]. The NiO nanoparticles exhibited a very small size of approximately 5 nm at a Ni sample with 3 nm thickness. The size and density of NiO nanoparticles are very low on the surface of nanowires decorated with a 3 nm thick Ni decoration. However, with increasing Ni thickness from 3 to 5 nm, the density and size of NiO nanoparticles increased. The NiO nanoparticles showed not a spherical but an irregular shape. This finding can be explained by the strong adhesion between deposited Ni and SnO_2. Thus, upon heat treatment, the Ni layer was partially melted and oxidised to form irregular shapes. Ni deposition formed no continuous layer covering the SnO_2 nanowires but incoherent nanoparticles. SEM observation showed the formation of NiO nanoparticles, whereas energy-dispersive X-ray spectroscopy analysis confirmed the composition of Si, Ni, O and Sn in the sample (Fig. S2, ESI†).

Further characteristics of the SnO_2 nanowires and NiO–SnO_2 nanowires were studied by TEM images (Fig. 3). Fig. 3(A) reveals low-magnification TEM image of bare SnO_2 nanowires featuring a smooth surface. The SnO_2 nanowires showed a single

crystallinity nature where clear lattice fringes are present [Fig. 3(B)]. The gap between adjacent lattice fringes is 0.33 nm, corresponding to the interspace of (110) plane of SnO_2.[37] Fig. 3(C) shows the surface of a SnO_2 nanowire after decoration with NiO nanoparticles. The NiO nanoparticles of approximately 10 nm were decorating homogenously the SnO_2 nanowires. Fig. 3(D) displays the high-magnification TEM image of SnO_2 nanowire decorated with NiO nanoparticles. The lattice fringes of SnO_2 is 0.33 nm. The NiO nanoparticles are highly crystalline, in which lattice fringes can be observed in with an interspace of 0.24 nm, corresponding to the distance between (111) atomic layers.[38]

H_2S is a toxic gas that is mainly present in biogas at relatively high concentrations at the ppm level. Thus, the sensing characteristics of fabricated sensors were measured at H_2S gas concentrations in the range of 1–10 ppm at different temperatures [Fig. 4–6]. Fig. 4 illustrates the transient resistance *versus* time upon exposure to different concentrations of H_2S measured at temperatures ranging from 200 °C to 350 °C of SnO_2 nanowire sensor decorated with 3 nm NiO. The base resistance of sensor at 200 °C in air was approximately 45 kΩ. Upon exposure to 10 ppm H_2S, the sensor resistance decreased to 13 kΩ with a response time of approximately 15 s [Fig. 4(A)]. When H_2S gas stopped flowing, the sensor resistance recovered to the initial value in a few minutes. With variation of H_2S concentrations from 10 ppm to 1 ppm, the sensor still exhibited good response characteristics, indicating the possibility of
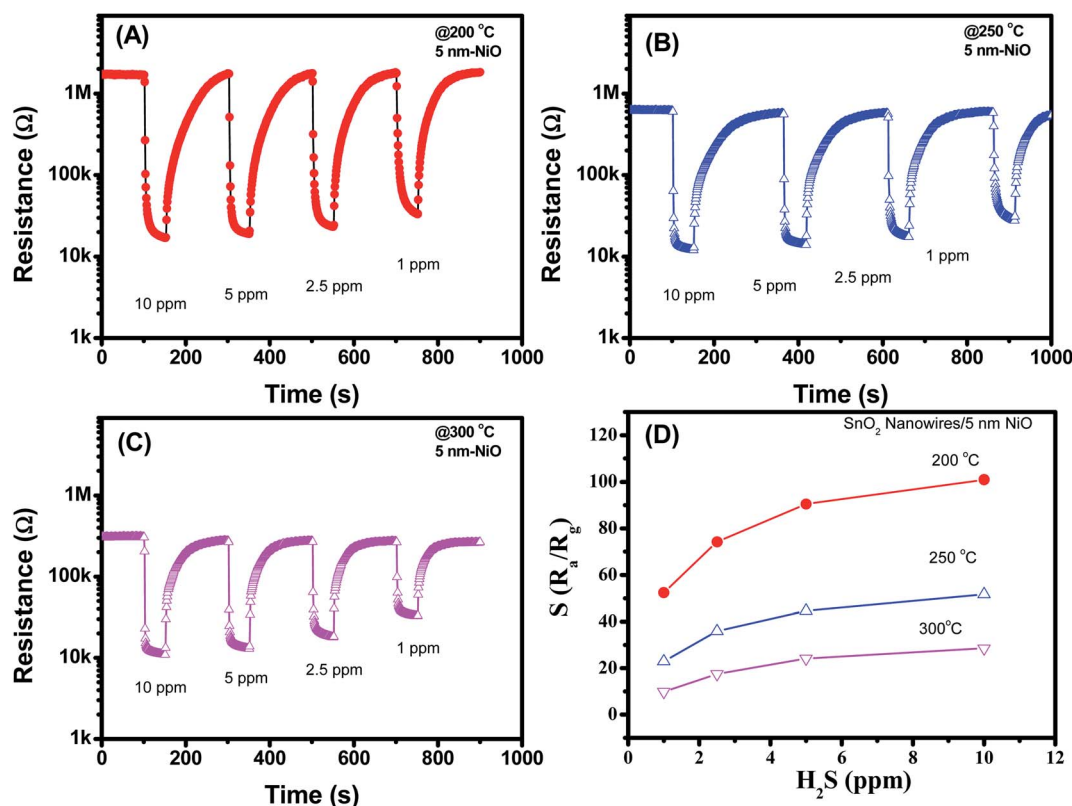

Fig. 5 H_2S sensing characteristics of SnO_2 nanowires decorated with NiO (5 nm) measured at different temperatures: (A) 200 °C; (B) 250 °C; (C) 300 °C; (D) sensor response as a function of H_2S concentration.

Fig. 6 H_2S sensing characteristics of SnO_2 nanowires decorated with NiO (10 nm) measured at different temperatures: (A) 200 °C; (B) 250 °C; (C) 300 °C; (D) sensor response as a function of H_2S concentration.
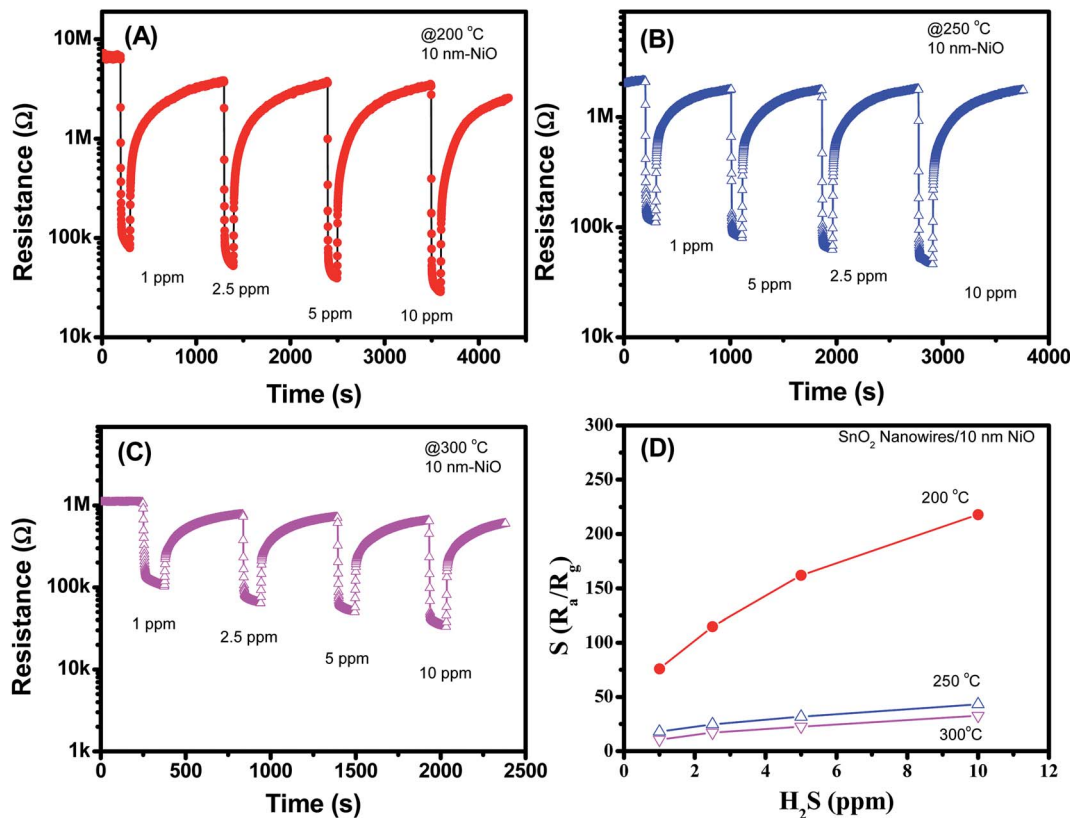
detection limit at the sub-ppm level. At a relatively high working temperature of approximately 250 °C, the sensor showed similar trend in response, that is, the resistance decreased significantly upon exposure to different H_2S gas. The response and recovery time of the sensor measured at 250 °C were 12 and 58 s, respectively. The response and recovery speeds of sensor improved with increased working temperature. At a high working temperature of 300 °C, the response and recovery time of the sensor approximated 6 and 35 s, respectively. Fig. 4(D) shows the sensor response as a function of H_2S concentration at different working temperatures. Sensor response increased linearly with the increase in H_2S concentrations from 1 ppm to 10 ppm. At a given H_2S concentration, the sensor response increased with increase in working temperature from 200 °C to 300 °C. The sensor response to 1 ppm H_2S was approximately 1.7 at 200 °C and increased to 2.1 and 2.7 with increasing working temperature to 250 °C and 300 °C, respectively. The sensor response improved, but it was still very low when considering that the response of bare SnO_2 nanowire-based sensor to 10 ppm H_2S at 300 °C approximated 3.2 (Fig. S3, ESI†).

Fig. 5(A–D) display the H_2S sensing characteristics of SnO_2 nanowires decorated with 5 nm NiO. The base resistance of the sensors at 200 °C in air was approximately 1.1 MΩ. This value is much higher than that of SnO_2 nanowires decorated with 3 nm NiO, indicating the enhanced depletion region at the interface between NiO and SnO_2. Upon exposure to H_2S gas, sensor

resistance decreased, similar to that of the sample decorated with 3 nm NiO. However, the sensor showed the highest response at a working temperature of 200 °C but not at 300 °C. This result implies that we can reduce the working temperature of SnO_2 nanowire sensors by increasing NiO thickness. In addition, the 5 nm NiO sensor response was relatively high, and the response to 1 ppm H_2S was approximately 56 at 200 °C. The sensor response increased from 56 to 100 with increasing H_2S concentration from 1 ppm to 10 ppm, indicating that the sensor was still unsaturated in the measured range.

Fig. 6(A–D) shows the H_2S sensing characteristics of SnO_2 nanowires decorated with 10 nm NiO. Further increase in the NiO thickness to 10 nm improved the sensor response, but a notably poor recovery characteristic was observed. Sensor resistance could not recover to the initial value after H_2S gas stopped flowing for 1000 s, thus limiting its reusability. The result is similar to that of 5 nm NiO sensor, possibly due to the strong reduction of NiO into NiS. In this case, we tested the H_2S response of the sensor to various H_2S concentrations at different temperatures and observed that the responses at 200 °C were the highest. The sensor response increases from 77 to 219 with increase of H_2S concentration from 1 to 10 ppm [Fig. 6(D)]. However, poor recovery characteristics can limit the practical applications of sensor.

Selectivity and stability of the sensor were studied for the 10 nm NiO sample, and the data are shown in Fig. 7. The data
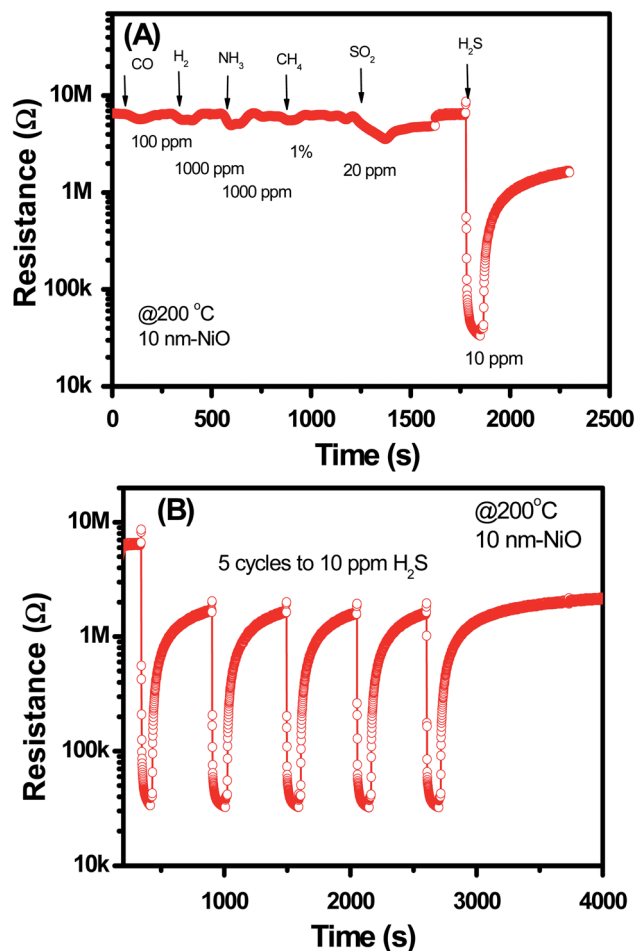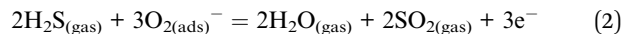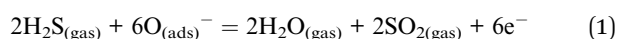
Fig. 7 (A) Selectivity and (B) stability of NiO–SnO$_2$ nanowire sensor measured at 200 °C.

demonstrates that the NiO–SnO$_2$ nanowire sensor has good selective response to H$_2$S among other gases including of CO, H$_2$, NH$_3$, CH$_4$, and SO$_2$ at measured temperature of 200 °C [Fig. 7(A)]. In addition, the sensor also showed good stability upon five cycles exposure to H$_2$S gas and back to air, as shown in Fig. 7(B). Such those results confirm that the NiO–SnO$_2$ nanowire sensor is effective for application in monitoring H$_2$S gas at low concentrations with high sensitivity and good selectivity.

Table 1 summarizes recent studies on sensing performance of H$_2$S gas sensors based on different materials. As can be seen, the pristine metal oxides showed low sensitivity to H$_2$S. However, by surface decoration, the sensor response was enhanced. Our sensor showed much higher response compared to others.

3.2 Gas sensing mechanism

Herein, sensor resistance decreased upon exposure to H$_2$S gas, indicating the increase in free electron in SnO$_2$. H$_2$S response is mainly based on the following reaction with pre-adsorbed oxygen species.[8]

$$2H_2S_{(gas)} + 6O_{(ads)}{}^- = 2H_2O_{(gas)} + 2SO_{2(gas)} + 6e^- \qquad (1)$$

$$2H_2S_{(gas)} + 3O_{2(ads)}{}^- = 2H_2O_{(gas)} + 2SO_{2(gas)} + 3e^- \qquad (2)$$

The released electrons contribute to increasing the main carriers in n-type SnO$_2$ semiconductor, thus decreasing sensor resistance. In addition, H$_2$S molecules can react with decorated NiO nanoparticles to form NiS upon exposure to H$_2$S gas. This reaction can occur easily at low temperature. Reaction with NiO results in the following:

$$H_2S_{(gas)} + NiO = H_2O_{(gas)} + NiS \qquad (3)$$
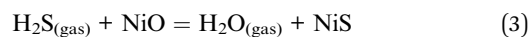
NiS shows a metallic behaviour[49] with a work function of 5.5 eV.[50] The conductivity of NiS can be expressed by the following equation:

$$\sigma = \frac{nq^2\tau}{m^*} \qquad (4)$$

where m^* refers to the effective mass of electrons in the material, n denotes electron density, and τ represents the average time between two collisions of electrons in the material crystal. The charge carrier density of NiS is approximately 3.67×10^{22} cm^3, and electron mobility is approximately 0.6 cm^2 V^{-1} s^{-1}.[49] The carrier density and hole mobility of NiO are 4.30×10^{10} cm^3 and 9.67×10^2 cm^2 V^{-1} s^{-1}, respectively.[51] The conductivity of NiO is much lower than that of NiS. Therefore, when exposed to H$_2$S gas, sulfidation of NiO to NiS reduced the sensor resistance. The SnO$_2$ nanowires feature a carrier density of the order of $n \approx 10^{16}$ cm^{-3} and mobility of $\mu \approx 70$ cm^2 V^{-1} s^{-1}.[52,53] Furthermore, the work function of SnO$_2$ nanowires is approximately 4.9 eV.[54] The work function of NiO varies from 5.23 eV to 6.43 eV (ref. 55) depending on the adsorbate gases, such as oxygen or carbon dioxide. The decoration of NiO on the surface of SnO$_2$ nanowire forms the p–n junction, modulating the conducting channel of nanowires.[56] The depletion region of p–n junction is calculated by the following equation:

$$W = \left[\frac{2\varepsilon_r\varepsilon_0}{q}\left(\frac{N_A + N_D}{N_A N_D}\right)\left(V_{bi\ p-n} - V\right)\right]^{1/2} \qquad (5)$$

where ε_r refers to the relative dielectric permittivity of the semiconductor, V_{bi} specifies the built-in voltage, and V denotes the applied bias. N_A and N_D represent the densities of ionised donors and acceptors, respectively. Upon exposure to H$_2$S, the NiO is sulphurised into NiS. As the work function of NiS (5.5 eV) is larger than that of n-type SnO$_2$ (4.9 eV), Schottky contact forms at the interface of SnO$_2$–NiS. The depletion width of the Schottky contact is calculated by the following equation:

$$W = \left[\frac{2\varepsilon_r\varepsilon_0}{q}\left(\frac{1}{N_D}\right)\left(V_{bi\ Schotkky} - V\right)\right]^{1/2} \qquad (6)$$

The barrier value of $V_{bi\ p-n}$ is approximately 1.2 eV, which is larger than the $V_{bi\ Schottky}$ value of approximately 0.6 eV. $N_A \approx 4.30 \times 10^{10}$ cm^3, $N_D \approx 10^{16}$ cm^{-3}. The width Schottky contact is smaller than that of the p–n junction, reducing the sensor resistance. Therefore, decoration of NiO on the surface of SnO$_2$ significantly increased the H$_2$S sensing performance of SnO$_2$ nanowires.

Table 1 A comparison data of our results and recent studies

No.	Materials	Working condition	$S = R_a/R_g$	Ref.
1	α-Fe_2O_3 nanochains	5 ppm H_2S @ 285 °C	5	39
2	α-Fe_2O_3 nanosheets	5 ppm H_2S at 135 °C	5.8	40
3	$ZnFe_2O_4$ nanoparticles	5 ppm H_2S at 135 °C	15.1	41
4	Porous $ZnFe_2O_4$ nanosheets	1 ppm H_2S at 85 °C	39.8	42
5	Fe_2O_3/ZnO nanoplates	100 ppm H_2S at 250 °C	130	43
6	NiO/ZnO nanowires	100 ppm H_2S at room temperature	~0.31	44
7	Au:Fe_2O_3 thin film	10 ppm H_2S at 250 °C	6.38	45
8	Ag-doped $CaCu_3Ti_4O_{12}$ films	10 ppm H_2S at 250 °C	100	46
9	Ni-doped $CaCu_3Ti_4O_{12}$ films	10 ppm H_2S at 250 °C	120	47
10	rGO/$ZnFe_2O_4$ nanofibers	1 ppm H_2S at 350 °C	147	8
11	Olive-shaped SnO_2 nanocrystals	10 ppm H_2S at 240 °C	120	48
12	NiO–SnO_2 nanowires	1 ppm H_2S at 200 °C	150	This study

4. Conclusion

We successfully decorated the surface of SnO_2 nanowires with NiO nanoparticles by electron beam evaporation. The density of NiO nanoparticles was controlled by varying the Ni thickness at 3, 5 and 10 nm. With effective decoration of NiO, the H_2S sensing characteristics of SnO_2 nanowires significantly improved by one or two orders. We also clarified the sensing mechanism of the sensor based on band structure, where the decoration of NiO nanoparticles on the surface of SnO_2 nanowires formed the p–n heterojunction and modulated the conducting channel of the nanowires. Such p–n heterojunctions are strongly sensitive to environmental H_2S gas, thereby improving the sensing performance.

Conflicts of interest

There are no conflicts to declare.

Acknowledgements

References

1 K. Lasko, K. P. Vadrevu and T. T. N. Nguyen, Analysis of air pollution over Hanoi, Vietnam using multi-satellite and MERRA reanalysis datasets, *PLoS One*, 2018, **13**, e0196629, DOI: 10.1371/journal.pone.0196629.

2 W. Pinate, D. Dangphonthong, S. Sirirach and S. Sukkhon, Removal of hydrogen sulfide (H_2S) from biogas for the community in the province of Maha Sarakham, *J. Phys.: Conf. Ser.*, 2017, **901**, 12049, DOI: 10.1088/1742-6596/901/1/012049.

3 T. K. V. Vu, D. Q. Vu, L. S. Jensen, S. G. Sommer and S. Bruun, Life Cycle Assessment of Biogas Production in Small-scale Household Digesters in Vietnam, *Asian-Australas. J. Anim. Sci.*, 2015, **28**, 716–729, DOI: 10.5713/ajas.14.0683.

4 N. Van Toan, N. V. Chien, N. Van Duy, D. D. Vuong, N. H. Lam, N. D. Hoa, N. Van Hieu and N. D. Chien, Scalable fabrication of SnO_2 thin films sensitized with CuO islands for enhanced H_2S gas sensing performance, *Appl. Surf. Sci.*, 2015, **324**, 280–285, DOI: 10.1016/j.apsusc.2014.10.134.

5 M. Turker, A. B. Baspinar and A. Hocalar, Monitoring and control of biogas desulphurization using oxidation reduction potential under denitrifying conditions, *J. Chem. Technol. Biotechnol.*, 2012, **87**, 682–688, DOI: 10.1002/jctb.2765.

6 D. Girardin, F. Berger, A. Chambaudet and R. Planade, Modelling of SO_2 detection by tin dioxide gas sensors, *Sens. Actuators, B*, 1997, **43**, 147–153, DOI: 10.1016/S0925-4005(97)00149-4.

7 Q. Zhou, W. Chen, J. Li, S. Peng, Z. Lu, Z. Yang and L. Xu, Highly Sensitive Hydrogen Sulfide Sensor Based on Titanium Dioxide Nanomaterials, *J. Nanoelectron. Optoelectron.*, 2018, **13**, 1784–1788, DOI: 10.1166/jno.2018.2417.

8 N. Van Hoang, C. M. Hung, N. D. Hoa, N. Van Duy and N. Van Hieu, Facile on-chip electrospinning of $ZnFe_2O_4$ nanofiber sensors with excellent sensing performance to H_2S down ppb level, *J. Hazard. Mater.*, 2018, **360**, 6–16, DOI: 10.1016/j.jhazmat.2018.07.084.

9 M. Bao, Y. Chen, F. Li, J. Ma, T. Lv, Y. Tang, L. Chen, Z. Xu and T. Wang, Plate-like p–n heterogeneous NiO/WO_3 nanocomposites for high performance room temperature NO_2 sensors, *Nanoscale*, 2014, **6**, 4063, DOI: 10.1039/c3nr05268k.

10 Q. Zhou, Q. Zhang, H. Liu, C. Hong, G. Wu, S. Peng, Q. Wang and D. Wu, Research on Gas Sensing Properties of Orthorhombic Molybdenum Oxide Based Sensor to Hydrogen Sulfide, *J. Nanoelectron. Optoelectron.*, 2017, **12**, 1072–1076, DOI: 10.1166/jno.2017.2119.

11 A. Mirzaei, S. S. Kim and H. W. Kim, Resistance-based H_2S gas sensors using metal oxide nanostructures: A review of recent advances, *J. Hazard. Mater.*, 2018, **357**, 314–331, DOI: 10.1016/j.jhazmat.2018.06.015.

12 Q. Zhou, L. Xu, A. Umar, W. Chen and R. Kumar, Pt nanoparticles decorated SnO_2 nanoneedles for efficient CO

gas sensing applications, *Sens. Actuators, B*, 2018, **256**, 656–664, DOI: 10.1016/j.snb.2017.09.206.

13 S. Zhang, P. Zhang, Y. Wang, Y. Ma, J. Zhong and X. Sun, Facile Fabrication of a Well-Ordered Porous Cu-Doped SnO$_2$ Thin Film for H$_2$S Sensing, *ACS Appl. Mater. Interfaces*, 2014, **6**, 14975–14980, DOI: 10.1021/am502671s.

14 P. M. Bulemo, H.-J. Cho, D.-H. Kim and I.-D. Kim, Facile Synthesis of Pt-Functionalized Meso/Macroporous SnO$_2$ Hollow Spheres through in Situ Templating with SiO$_2$ for H$_2$S Sensors, *ACS Appl. Mater. Interfaces*, 2018, **10**, 18183–18191, DOI: 10.1021/acsami.8b00901.

15 I.-S. Hwang, J.-K. Choi, S.-J. Kim, K.-Y. Dong, J.-H. Kwon, B.-K. Ju and J.-H. Lee, Enhanced H$_2$S sensing characteristics of SnO$_2$ nanowires functionalized with CuO, *Sens. Actuators, B*, 2009, **142**, 105–110, DOI: 10.1016/j.snb.2009.07.052.

16 Z. Song, J. Liu, Q. Liu, H. Yu, W. Zhang, Y. Wang, Z. Huang, J. Zang and H. Liu, Enhanced H$_2$S gas sensing properties based on SnO$_2$ quantum wire/reduced graphene oxide nanocomposites: Equilibrium and kinetics modeling, *Sens. Actuators, B*, 2017, **249**, 632–638, DOI: 10.1016/j.snb.2017.04.023.

17 Q. Zhou, W. Chen, L. Xu, R. Kumar, Y. Gui, Z. Zhao, C. Tang and S. Zhu, Highly sensitive carbon monoxide (CO) gas sensors based on Ni and Zn doped SnO$_2$ nanomaterials, *Ceram. Int.*, 2018, **44**, 4392–4399, DOI: 10.1016/j.ceramint.2017.12.038.

18 T. Itoh, T. Nakashima, T. Akamatsu, N. Izu and W. Shin, Nonanal gas sensing properties of platinum, palladium, and gold-loaded tin oxide VOCs sensors, *Sens. Actuators, B*, 2013, **187**, 135–141, DOI: 10.1016/j.snb.2012.09.097.

19 P. Van Tong, N. D. Hoa, N. Van Duy, D. T. T. Le and N. Van Hieu, Enhancement of gas-sensing characteristics of hydrothermally synthesized WO$_3$ nanorods by surface decoration with Pd nanoparticles, *Sens. Actuators, B*, 2016, **223**, 453–460, DOI: 10.1016/j.snb.2015.09.108.

20 J. Gong, Q. Chen, M.-R. Lian, N.-C. Liu, R. G. Stevenson and F. Adami, Micromachined nanocrystalline silver doped SnO$_2$ H$_2$S sensor, *Sens. Actuators, B*, 2006, **114**, 32–39, DOI: 10.1016/j.snb.2005.04.035.

21 X. Liu, B. Du, Y. Sun, M. Yu, Y. Yin, W. Tang, C. Chen, L. Sun, B. Yang, W. Cao and M. N. R. Ashfold, Sensitive Room Temperature Photoluminescence-Based Sensing of H$_2$S with Novel CuO–ZnO Nanorods, *ACS Appl. Mater. Interfaces*, 2016, **8**, 16379–16385, DOI: 10.1021/acsami.6b02455.

22 M. N. Rumyantseva, S. A. Vladimirova, N. A. Vorobyeva, I. Giebelhaus, S. Mathur, A. S. Chizhov, N. O. Khmelevsky, A. Y. Aksenenko, V. F. Kozlovsky, O. M. Karakulina, J. Hadermann, A. M. Abakumov and A. M. Gaskov, p-CoO$_x$/n-SnO$_2$ nanostructures: New highly selective materials for H$_2$S detection, *Sens. Actuators, B*, 2018, **255**, 564–571, DOI: 10.1016/j.snb.2017.08.096.

23 N. Van Toan, N. V. Chien, N. Van Duy, D. D. Vuong, N. H. Lam, N. D. Hoa, N. Van Hieu and N. D. Chien, Scalable fabrication of SnO$_2$ thin films sensitized with CuO islands for enhanced H$_2$S gas sensing performance, *Appl.*

24 N. D. Hoa, D. Van Thien, N. Van Duy and N. Van Hieu, Facile synthesis of single-crystal nanoporous α-NiS nanosheets from Ni(OH)$_2$ counterpart, *Mater. Lett.*, 2015, **161**, 282–285, DOI: 10.1016/j.matlet.2015.08.123.

25 M. Kaur, B. K. Dadhich, R. Singh, K. Ganapathi, T. Bagwaiya, S. Bhattacharya, A. K. Debnath, K. P. Muthe and S. C. Gadkari, RF sputtered SnO$_2$:NiO thin films as sub-ppm H$_2$S sensor operable at room temperature, *Sens. Actuators, B*, 2017, **242**, 389–403, DOI: 10.1016/j.snb.2016.11.054.

26 N. Van Hieu, P. Thi Hong Van, L. Tien Nhan, N. Van Duy and N. Duc Hoa, Giant enhancement of H$_2$S gas response by decorating n-type SnO$_2$ nanowires with p-type NiO nanoparticles, *Appl. Phys. Lett.*, 2012, **101**, 253106, DOI: 10.1063/1.4772488.

27 S. Lee, S. Kim, B. Hwang, S. Jung, D. Ragupathy, I. Son, D. Lee and J. Kim, Improvement of H$_2$S Sensing Properties of SnO$_2$-Based Thick Film Gas Sensors Promoted with MoO$_3$ and NiO, *Sensors*, 2013, **13**, 3889–3901, DOI: 10.3390/s130303889.

28 Y. Wang, H. Zhang and X. Sun, Electrospun nanowebs of NiO/SnO$_2$ p–n heterojunctions for enhanced gas sensing, *Appl. Surf. Sci.*, 2016, **389**, 514–520, DOI: 10.1016/j.apsusc.2016.07.073.

29 A. Martucci, D. Buso, M. De Monte, M. Guglielmi, C. Cantalini and C. Sada, Nanostructured sol–gel silica thin films doped with NiO and SnO$_2$ for gas sensing applications, *J. Mater. Chem.*, 2004, **14**, 2889–2895, DOI: 10.1039/B405301J.

30 C. Wei, B. Bo, F. Tao, Y. Lu, S. Peng, W. Song and Q. Zhou, Hydrothermal Synthesis and Structural Characterization of NiO/SnO$_2$ Composites and Hydrogen Sensing Properties, *J. Spectrosc.*, 2015, **2015**, 450485.

31 H. Gao, L. Zhao, L. Wang, P. Sun, H. Lu, F. Liu, X. Chuai and G. Lu, Ultrasensitive and low detection limit of toluene gas sensor based on SnO$_2$-decorated NiO nanostructure, *Sens. Actuators, B*, 2018, **255**, 3505–3515, DOI: 10.1016/j.snb.2017.09.184.

32 D. D. Trung, N. D. Hoa, P. Van Tong, N. Van Duy, T. D. Dao, H. V. Chung, T. Nagao and N. Van Hieu, Effective decoration of Pd nanoparticles on the surface of SnO$_2$ nanowires for enhancement of CO gas-sensing performance, *J. Hazard. Mater.*, 2014, **265**, 124–132, DOI: 10.1016/j.jhazmat.2013.11.054.

33 J. Fang, Y. Zhu, D. Wu, C. Zhang, S. Xu, D. Xiong, P. Yang, L. Wang and P. K. Chu, Gas sensing properties of NiO/SnO$_2$ heterojunction thin film, *Sens. Actuators, B*, 2017, **252**, 1163–1168, DOI: 10.1016/j.snb.2017.07.013.

34 D. R. Sahu, T.-J. Wu, S.-C. Wang and J.-L. Huang, Electrochromic behavior of NiO film prepared by e-beam evaporation, *Journal of Science: Advanced Materials and Devices*, 2017, **2**, 225–232, DOI: 10.1016/j.jsamd.2017.05.001.

35 K. Nguyen, C. M. Hung, T. M. Ngoc, D. T. Thanh Le, D. H. Nguyen, D. Nguyen Van and H. Nguyen Van, Low-temperature prototype hydrogen sensors using Pd-

decorated SnO₂ nanowires for exhaled breath applications, *Sens. Actuators, B*, 2017, **253**, 156–163, DOI: 10.1016/j.snb.2017.06.141.

36 N. D. Hoa, C. M. Hung, N. Van Duy and N. Van Hieu, Nanoporous and crystal evolution in nickel oxide nanosheets for enhanced gas-sensing performance, *Sens. Actuators, B*, 2018, **273**, 784–793, DOI: 10.1016/j.snb.2018.06.095.

37 S. Wang, G. Cheng, K. Cheng, X. Jiang and Z. Du, The current image of single SnO₂ nanobelt nanodevice studied by conductive atomic force microscopy, *Nanoscale Res. Lett.*, 2011, **6**, 541, DOI: 10.1186/1556-276X-6-541.

38 Y. Zhu, C. Cao, S. Tao, W. Chu, Z. Wu and Y. Li, Ultrathin Nickel Hydroxide and Oxide Nanosheets: Synthesis, Characterizations and Excellent Supercapacitor Performances, *Sci. Rep.*, 2015, **4**, 5787, DOI: 10.1038/srep05787.

39 J. Ma, L. Mei, Y. Chen, Q. Li, T. Wang, Z. Xu, X. Duan and W. Zheng, α-Fe₂O₃ nanochains: ammonium acetate-based ionothermal synthesis and ultrasensitive sensors for low-ppm-level H₂S gas, *Nanoscale*, 2013, **5**, 895–898, DOI: 10.1039/C2NR33201A.

40 H.-J. Zhang, F.-N. Meng, L.-Z. Liu and Y.-J. Chen, Convenient route for synthesis of alpha-Fe₂O₃ and sensors for H₂S gas, *J. Alloys Compd.*, 2019, **774**, 1181–1188, DOI: 10.1016/j.jallcom.2018.09.384.

41 H.-J. Zhang, F.-N. Meng, L.-Z. Liu, Y.-J. Chen and P.-J. Wang, Highly sensitive H₂S sensor based on solvothermally prepared spinel ZnFe₂O₄ nanoparticles, *J. Alloys Compd.*, 2018, **764**, 147–154, DOI: 10.1016/j.jallcom.2018.06.052.

42 X. Gao, Y. Sun, C. Zhu, C. Li, Q. Ouyang and Y. Chen, Highly sensitive and selective H2S sensor based on porous ZnFe₂O₄ nanosheets, *Sens. Actuators, B*, 2017, **246**, 662–672, DOI: 10.1016/j.snb.2017.02.100.

43 K. Fan, J. Guo, L. Cha, Q. Chen and J. Ma, Atomic layer deposition of ZnO onto Fe₂O₃ nanoplates for enhanced H₂S sensing, *J. Alloys Compd.*, 2017, **698**, 336–340, DOI: 10.1016/j.jallcom.2016.12.203.

44 Z. Qu, Y. Fu, B. Yu, P. Deng, L. Xing and X. Xue, High and fast H₂S response of NiO/ZnO nanowire nanogenerator as a self-powered gas sensor, *Sens. Actuators, B*, 2016, **222**, 78–86, DOI: 10.1016/j.snb.2015.08.058.

45 V. Balouria, N. S. Ramgir, A. Singh, A. K. Debnath, A. Mahajan, R. K. Bedi, D. K. Aswal and S. K. Gupta, Enhanced H₂S sensing characteristics of Au modified Fe₂O₃ thin films, *Sens. Actuators, B*, 2015, **219**, 125–132, DOI: 10.1016/j.snb.2015.04.113.

46 A. Natkaeo, D. Phokharatkul, J. H. Hodak, A. Wisitsoraat and S. K. Hodak, Highly selective sub–10 ppm H₂S gas sensors based on Ag-doped CaCu₃Ti₄O₁₂ films, *Sens. Actuators, B*, 2018, **260**, 571–580, DOI: 10.1016/j.snb.2017.12.134.

47 A. Boontum, D. Phokharatkul, J. H. Hodak, A. Wisitsoraat and S. K. Hodak, H₂S sensing characteristics of Ni-doped CaCu₃Ti₄O₁₂ films synthesized by a sol-gel method, *Sens. Actuators, B*, 2018, **260**, 877–887, DOI: 10.1016/j.snb.2018.01.090.

48 J. Hu, G. Yin, J. Chen, M. Ge, J. Lu, Z. Yang and D. He, An olive-shaped SnO₂ nanocrystal-based low concentration H 2 S gas sensor with high sensitivity and selectivity, *Phys. Chem. Chem. Phys.*, 2015, **17**, 20537–20542, DOI: 10.1039/C5CP02854J.

49 R. Boughalmi, R. Rahmani, A. Boukhachem, B. Amrani, K. Driss-Khodja and M. Amlouk, Metallic behavior of NiS thin film under the structural, optical, electrical and ab initio investigation frameworks, *Mater. Chem. Phys.*, 2015, **163**, 99–106, DOI: 10.1016/j.matchemphys.2015.07.019.

50 X. Wang, B. Batter, Y. Xie, K. Pan, Y. Liao, C. Lv, M. Li, S. Sui and H. Fu, Highly crystalline, small sized, monodisperse α-NiS nanocrystal ink as an efficient counter electrode for dye-sensitized solar cells, *J. Mater. Chem. A*, 2015, **3**, 15905–15912, DOI: 10.1039/C5TA02946E.

51 E. S. Hassan, A. A. Saeed and A. K. Elttayef, Doping and thickness variation influence on the structural and sensing properties of NiO film prepared by RF-magnetron sputtering, *J. Mater. Sci.: Mater. Electron.*, 2016, **27**, 1270–1277, DOI: 10.1007/s10854-015-3885-3.

52 D. Tsokkou, A. Othonos and M. Zervos, Carrier dynamics and conductivity of SnO₂ nanowires investigated by time-resolved terahertz spectroscopy, *Appl. Phys. Lett.*, 2012, **100**, 133101, DOI: 10.1063/1.3698097.

53 S. Sub Kim, H. Gil Na, H. Woo Kim, V. Kulish and P. Wu, Promotion of acceptor formation in SnO₂ nanowires by e-beam bombardment and impacts to sensor application, *Sci. Rep.*, 2015, **5**, 10723, DOI: 10.1038/srep10723.

54 R. Könenkamp, R. C. Word and M. Godinez, Electroluminescence in nanoporous TiO₂ solid-state heterojunctions, *Nanotechnology*, 2006, **17**, 1858–1861, DOI: 10.1088/0957-4484/17/8/008.

55 M. T. Greiner, M. G. Helander, Z.-B. Wang, W.-M. Tang and Z.-H. Lu, Effects of Processing Conditions on the Work Function and Energy-Level Alignment of NiO Thin Films, *J. Phys. Chem. C*, 2010, **114**, 19777–19781, DOI: 10.1021/jp108281m.

56 G. Zhang, X. Han, W. Bian, J. Zhan and X. Ma, Facile synthesis and high formaldehyde-sensing performance of NiO–SnO₂ hybrid nanospheres, *RSC Adv.*, 2016, **6**, 3919–3926, DOI: 10.1039/C5RA21063A.